JOURNAL OF CATALYSIS 46, 214–224 (1977)

Diffusivity and Structure of Porous Pellets

DEJAN DJ. SMILJANIĆ

Department of Catalysis, Institute for Chemistry, Technology and Metallurgy, Belgrade, Yugoslavia

Received August 18, 1975; revised October 13, 1976

The permeability measurement method has been used to estimate effective diffusivities in four samples of catalysts (three commercial and one prepared in the laboratory). Useful correlation between the diffusivity and porosity of each pellet of the sample has been established by applying a comparatively simple model of porous structure. The application of the model to literature data also gave satisfactory results. Some apparent inconsistencies in results of recent diffusion experiments have been explained through the variation of the labyrinth factor from pellet to pellet of the sample.

NOMENCLATURE

a	Edge of elementary cell (cm)
a_{keff}	Effective dimension of the square channel for Knudsen diffusion (cm)
a_{neff}	The same as a_{keff}, but for normal diffusion (cm)
b	Diameter of the cylindrical pellet (cm)
d	True density of the pellet (g/cm³)
D_{12}	Theoretical normal diffusivity (cm²/s)
D_{12eff}	Effective normal diffusivity (cm²/s)
D_{kR}	Knudsen diffusivity, with R as linear dimension of the pore (cm²/s)
$D_{k\rho}$	The same as D_{kR}, but with ρ as linear dimension (cm²/s)
$\bar{D}_k$	Average Knudsen diffusivity in the pore, after the model (cm²/s)
D_{keff}	Effective Knudsen diffusivity (cm²/s)
$D_{k\,exp}$	Experimentally measured value of D_{keff} (cm²/s)
g	Weight of the cylindrical pellet (g)
l	Length of the cylindrical pellet (cm)
M	Molecular weight (g/mol)
n	Dimensionless parameter ($=\rho/R$)
p	Pressure (Torr)
Δp_0	Pressure difference at the start of diffusivity measurement (Torr)
$\Delta p(t)$	Pressure difference after a time t from the start of diffusivity measurement (Torr)
$P(p)$	Permeability of the pellet as a function of pressure p (cm²/s)
R	Side of the square cross section of connecting pore, after the model (cm)
$S(i)$	Standard deviation of the parameter i
t	Time (s)
T	Absolute temperature (°K)
$V(i)$	Variation coefficient of the parameter i (%)
V	Volume of the cylindrical pellet (cm³)
V_1, V_2	Gas volumes A and B (Fig. 1)
X_i	denotes $R_i - R_0$ or $\rho_i - \rho_0$ (see text)
δX_i	Dimensionless parameter ($=X_i/R_0$)
γ	Apparent density of the pellet (g/cm³)

ISSN 0021-9517

θ Porosity (dimensionless)
θ_{keff} Free surface porosity for Knudsen diffusion (dimensionless)
λ_T Theoretical labyrinth factor for Knudsen diffusion, after the model $(=D_{keff}/\bar{D}_k)$
λ_T' Practical labyrinth factor $(=D_{keff}/D_{kR})$
λ_{exp}' Experimentally obtained λ_T' $(=D_{k\,exp}/D_{kR})$
λ_n Theoretical labyrinth factor for normal diffusion, after the model $(=D_{12eff}/D_{12})$
ρ Edge of the cubical central pore, after the model (cm)
τ Tortuosity factor (dimensionless)
ω Dimensionless parameter $(=R/a)$
Δi Absolute error of measurement of the quantity i
0 Index denotes the mean value of the corresponding parameter
i Index denotes the value of corresponding parameter, other than the mean value.

INTRODUCTION

The effective diffusivity of a porous catalyst pellet is the property which should describe the features of the pore structure in such a way that meaningful speculations can be made about the activity, selectivity and poisoning characteristics, connecting in this way the fundamental and practical aspects of the catalyst behavior. Although many models to predict effective diffusivities have been described (*1–8*), no universal model has yet been developed, as pointed out by Satterfield (*9*). The best models predict effective diffusivities only within a factor of two. This low precision, although probably sufficient for approximate technical calculations, illustrates the inadequacy of our knowledge about the fundamental phenomena inside the porous structure, i.e., about the processes at the microscopic level.

The following difficulties arise when comparing the models so far published:

1. In many cases, the model development has been based on investigation of a limited number of porous materials, chiefly catalysts; it must be admitted that such models represent the particular materials very well, but extrapolation to other materials is, often, very poor (*10*).

2. The standard Wicke–Kallenbach technique (*11*), when used with pressures not too much higher than atmospheric, gives results which often fall in the transient region between Knudsen and bulk diffusion, due to the width of the pore volume distribution of the sample; or, if the pore volume distribution appears bimodal, the diffusion process is some combination of the two limiting modes. These phenomena obviously increase the uncertainty of conclusions drawn.

3. Studies made using several pellets in one experiment forces the direct use of mean values, leaving the very nature of "micro-phenomena" unresolved. As shown elsewhere (*12*), the porosity variation from pellet to pellet in some cases exceeds 10%, which could be one of the primary reasons for distortion of experimental results.

In view of these objections, we decided to perform experiments in the Knudsen region, or very close to it, using only one pellet in any given experiment. Thus, the aim of present paper is not to develop a "better" model with increased predictability, but to clarify certain processes which take part in the genesis of a porous pellet and influence the effective diffusivity.

EXPERIMENTAL PROCEDURES

Materials

Four catalysts have been studied in this work. The first three were commercial catalysts for SO_2-oxidation (Topsøe VK-7), methanol synthesis (Topsøe SMK) and water gas shift reaction (Topsøe SK), respectively, and the fourth was a water gas shift catalyst (Ž-46) prepared in our laboratory.

All samples were in the form of cylindrical tablets. This choice has been made for two reasons. First, it is easy to measure with sufficient accuracy the external dimensions of cylinders, and second, the investigation of extruded samples revealed irregular cracks, sometimes almost invisible, which distorted results. So extruded samples have been excluded from the investigation.

Methods

The true density has been determined pycnometrically using benzene as a liquid. To exclude the effect of totally dead pores, not contributing to diffusion in the steady state, pellets have not been ground. The true density has been assumed to be constant for each sample. The precision of the true density measurement has been proved to be inside 1%.

The apparent density has been determined for each pellet by exact measurement of its weight (to 0.1 mg) and dimensions (to 0.05 mm).

Two commercial mercury porosimeters (Aminco Winslow, 5000 psi; Carlo Erba Model 70, 2000 at) have been used for determination of the pore volume distribution. The pellets have not been ground.

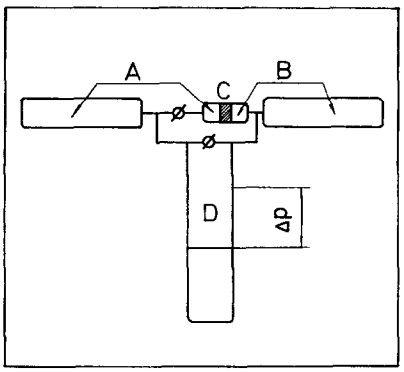

FIG. 1. Scheme of apparatus for measurement of effective Knudsen diffusivities. (A, B) gas volumes; (C) porous pellet; (D) differential mercury manometer.

TABLE 1

Textural Properties of the Investigated Materials

No.	Sample	d (g/cm³)	γ_0 (g/cm³)	θ_0 (macro)	θ_0 (micro)
1	Topsøe VK7	2.50	1.35	0.458	—
2	Topsøe SMK	3.59	2.44	0.321	—
3	Topsøe SK	3.76	2.00	0.140	0.327[a]
4	Ž-46	4.93	1.32	0.736	—

[a] Differentiation between micro- and macroporosity has been made for this sample only, because of clear bidisperse distribution. Partition pore diameter was 500 Å.

Effective diffusivity has been determined by the use of the modified method of Villet and Wilhelm (*13*), adapted for porous pellets (*14*).

The scheme of the apparatus is shown in Fig. 1. It consists of two gas volumes A and B, separated by a porous pellet C. Close to the base of the pellet is attached a mercury U-manometer D. The procedure is the following: the whole apparatus has been evacuated at room temperature to 0.01 Torr for 2 hr and washed twice with nitrogen. After the last evacuation a certain pressure difference of nitrogen, Δp_0, is established between the volumes A and B, and then its decrease as a function of time, $\Delta p(t)$, was measured. In this way we obtained the permeability at the mean absolute pressure p_1: $P(p_1)$. We obtained another permeability at some other mean pressure p_2: $P(p_2)$, and now, extrapolating permeability to zero pressure, we obtained D_{keff} as the intercept of the straight line on the $P(p)$ axis, when drawn in the coordinates $P(p)$–p, for the given pellet and nitrogen. All measurements have been made at room temperature (ca. 20°C). The details of the method are presented elsewhere (*14*).

The method assumes that the total flow through the pellet under the pressure gradient is the sum of Knudsen flow, independent of absolute pressure, and viscous flow, directly proportional to absolute pressure. Very nearly, this is true (*15*, *16*); moreover, as can be seen from the following

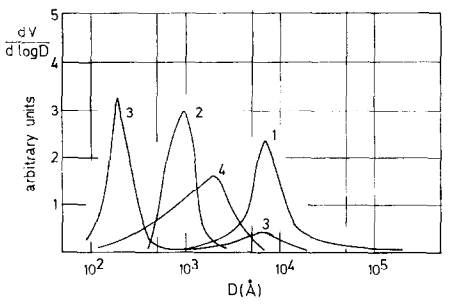

FIG. 2. Pore volume distribution curves for investigated samples. (1) Topsøe VK-7; (2) Topsøe SMK; (3) Topsøe SK; (4) Ž-46.

text, the need for absolute accuracy is not the point of this work.

Now, we must emphasize one essential technical detail, namely, the sealing of the pellet, supposing that it has troubled other experimenters, too. The procedure for this was as follows: a mold in the form of a ring was made of transparent tracing linen. The mold was set on a piece of the same linen, with the pellet in the center. Red sealing wax, melted in a crucible was then poured into the mold. After cooling the mold was removed and visual inspection

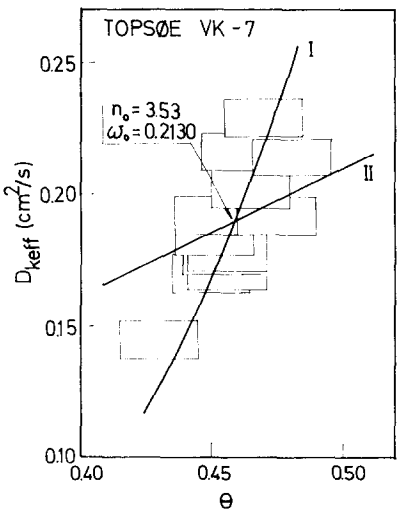

FIG. 3. Plot of effective nitrogen Knudsen diffusivity vs total porosity for Topsøe VK-7. (I, II) curves calculated for cases I and II, respectively (see text).

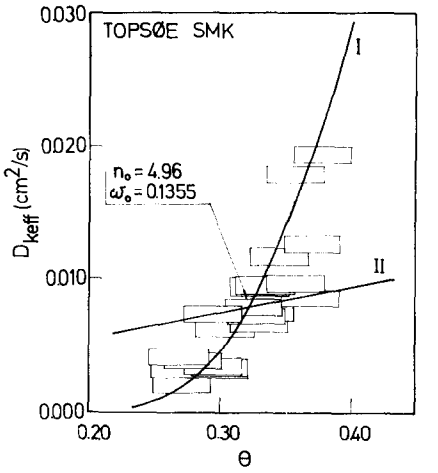

FIG. 4. Plot of effective nitrogen Knudsen diffusivity vs total porosity for Topsøe SMK. (I, II) curves calculated for cases I and II, respectively (see text).

was made; repairs were made with a hot needle. Then, the end of the glass tube (pellet carrier) was heated on the burner and pressed into the wax around the pellet. This procedure provided perfect sealing. In any cases of doubtful sealing of the pellet, new repairs were made after the diffusivity measurement; the measurement was repeated and the first result was compared with the second.

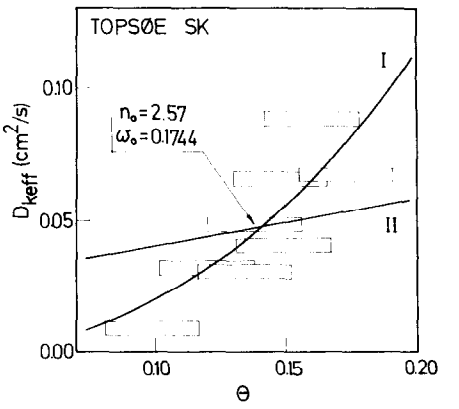

FIG. 5. Plot of effective nitrogen Knudsen diffusivity vs macroporosity for Topsøe SK. (I, II) curves calculated for cases I and II, respectively (see text).

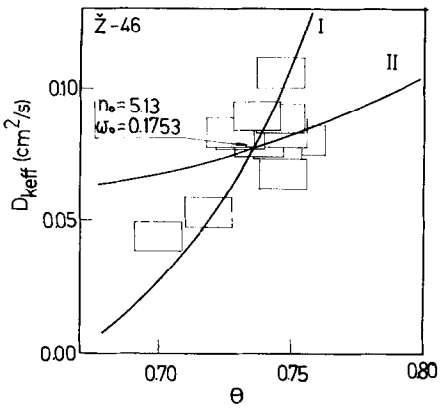

FIG. 6. Plot of effective nitrogen Knudsen diffusivity vs total porosity for Ž-46. (I, II) curves calculated for cases I and II, respectively (see text).

Considering the accuracy of the determination of θ and D_{keff} we may proceed as follows: Eqs. (1) and (2) express porosity and permeability (*14*) as functions of the directly measurable properties:

$$\theta = 1 - \frac{\gamma}{d} = 1 - \frac{g}{(b^2\bar{u}/4)\cdot l\cdot d}, \qquad (1)$$

$$P(p_i) = \frac{1}{(1/V_1) + (1/V_2)} \cdot \frac{l}{(b^2\bar{u}/4)\cdot t} \times \ln\left(\frac{\Delta p_0}{\Delta p(t)}\right). \qquad (2)$$

When we introduce in Eq. (2) the actual quantities, i.e., $V_1 = 546$ cm³, $V_2 = 453$ cm³, we obtain

$$P(p_i) = 727\,\frac{l}{b^2\cdot t}\log\left(\frac{\Delta p_0}{\Delta p(t)}\right). \qquad (2')$$

The limits of absolute error for θ and D_{keff}, according to the rules of the theory of errors, are the following:

$$\Delta\theta = (1-\theta)\left(\frac{\Delta g}{g} + \frac{\Delta l}{l} + 2\frac{\Delta b}{b} + \frac{\Delta d}{d}\right), \qquad (3)$$

$$\Delta D_{keff} = D_{keff}\left\{\frac{\Delta l}{l} + 2\frac{\Delta b}{b} + \frac{\Delta t}{t} + \frac{0.4343}{\log\left(\frac{\Delta p_0}{\Delta p(t)}\right)}\left[\frac{\Delta(\Delta p_0)}{\Delta p_0} + \frac{\Delta[\Delta p(t)]}{\Delta p(t)}\right]\right\}. \qquad (4)$$

We assumed that the form of the Eq. (4) is valid both for permeability and D_{keff}, which is true for the precision of the determination. In Figs. 3, 4, 5 and 6 every experimental point is surrounded with a rectangle, the sides of which represent $\Delta\theta$ and ΔD_{keff}, respectively.

RESULTS AND DISCUSSION

The texture properties of these samples are shown in Table 1 and Fig. 2.

The results of diffusivity measurement for all samples are shown in Figs. 3, 4, 5, and 6 in coordinates D_{keff}–θ. (For Topsøe SK, the correlation has been made with macroporosity.)

Now, we can confirm the clear relation between D_{keff} and θ for each sample. Comparing the results of four samples, we note in addition that D_{keff} is not unequivocally defined through the mean value of porosity, i.e., the diffusivity is not a single monotonic function of porosity.

This conclusion is not at all new. We point it out only to make evident the need

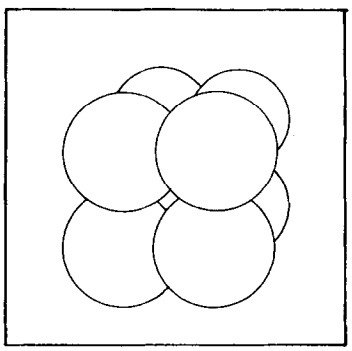

FIG. 7. Arrangement of primary particles inside a porous pellet, after the model.

of taking into consideration other parameters besides porosity. In this paper we mention some of these parameters.

Starting in our reasoning from the known methods of preparation of catalysts and catalyst supports, we assumed a concept very close to the ideas of other authors (*1*, *6*, *17*) in that we imagine the porous pellet to be composed of primary particles, the geometrical dimensions of which do not differ substantially. Primary particles, being pressed together, leave channels in between, with a cross section of variable magnitude, which form a continuous space, Fig. 7. We proceed by assuming that the whole structure is formed through the repeating of elementary cells (Fig. 8), equal to each other, and regularly put together. The elementary cell is the cube with edge a, having a cubical central pore (edge ρ) and six pores with square cross section (R^2), connecting the central pore with the centers of the sides of the elementary cell. Diffusion flux is parallel to the arrow (perpendicular to one of the cube sides).

The choice of the square cross section is made for the sake of simple calculation; finally, according to Satterfield (*18*) the model details are of minor importance compared to the significance of cross section ratio.

The model, simply imagined in this way, can be totally defined using three parameters: a, R and ρ, or with convenient transformation: R, $\omega = R/a$ and $n = \rho/R$. The permitted values of n range from 1 to ∞, and of ω, from 0 to $1/n$.

The total porosity of such a system, defined through the dimensionless parameters ω and n is:

$$\theta = \frac{\rho^3 + 3(a-\rho)R^2}{a^3} = \omega^2[3 + (n^3 - 3n)\omega]. \quad (5)$$

The average diffusivity in the pores of this system can be defined as the sum of flow impedances (*19*):

$$\frac{a}{a_{keff}^2 \bar{D}_k} = \frac{a-\rho}{R^2 D_{kR}} + \frac{\rho}{\rho^2 D_{k\rho}}, \quad (6)$$

from where we obtain the "effective dimension of a square channel" for Knudsen diffusion:

$$\left(\frac{R}{a_{keff}}\right)^3 = 1 - \omega\left(n - \frac{1}{n^2}\right). \quad (7)$$

This calculation has not taken into account the pores which are in the plane perpendicular to the flow, which do not contribute to the flux through the cell.

The effective Knudsen diffusivity across the cell is defined by:

$$D_{keff} = \lambda_T \cdot \bar{D}_k. \quad (8)$$

On the other side, the labyrinth factor may be defined as the ratio of surface porosity for Knudsen diffusion and tortuosity factor; for our model we obtain:

$$\lambda_T = \frac{\theta_{keff}}{\tau} = \frac{\theta_{keff}}{1} = \left(\frac{a_{keff}}{a}\right)^2. \quad (9)$$

(According to the model $\tau = 1$, and the free area for Knudsen diffusion is a_{keff}^2.)

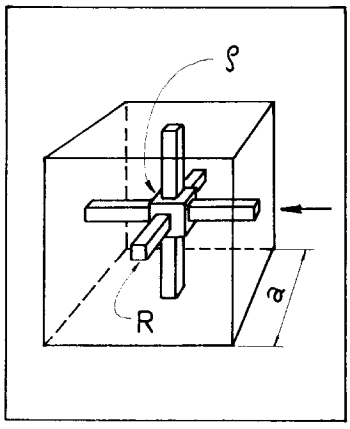

FIG. 8. Elementary cell, according to the model presented. (a) Edge of the elementary cell; (ρ) edge of the central cubical pore; (R) side of the square cross section of the connecting pore; diffusion flux is parallel to the arrow.

The verification of the model requires, however, the experimental determination of a_{keff} and a, i.e., the measurement of the model parameters R, ω, and n. Unfortunately, at present this is not possible.

According to some authors (*20*), the mercury penetration method offers only the value for R with enough probability, so we are forced to introduce practical parameters D_{kR} and λ_T', defined as follows:

$$D_{kR} = 4850 \cdot R(T/M)^{\frac{1}{2}}, \tag{10}$$

$$\lambda_T' = \frac{D_{keff}}{D_{kR}} = \frac{D_{keff}}{\bar{D}_k} \cdot \frac{\bar{D}_k}{D_{kR}} = \lambda_T \cdot \frac{a_{keff}}{R}. \tag{11}$$

Hence

$$\lambda_T' = \left(\frac{a_{keff}}{a}\right)^2 \frac{a_{keff}}{R} = \frac{\omega^2}{1 - [n - (1/n^2)]\omega}. \tag{12}$$

Manipulating the experimental results, we use consequently the most probable diameter from the pore-volume distribution as the value for R, without regard to the fact that the mercury penetration method has been developed for pores of circular cross section.

From this R we calculate D_{kR} and λ_{exp}', defined as:

$$\lambda_{exp}' = \frac{D_{k\,exp}}{D_{kR}}. \tag{13}$$

Now, λ_{exp}' can be compared with λ_T'. Combining Eqs. (5) and (12) through the elimination of ω, we obtained the very complicated but explicit expression:

$$\theta = \left\{\left[\left(n - \frac{1}{n^2}\right)^2 \frac{\lambda_T'^2}{4} + \lambda_T'\right]^{\frac{1}{2}} - \frac{\lambda_T'}{2}\left(n - \frac{1}{n^2}\right)\right\}^2 \cdot \left(3 + (n^3 - 3n) \times \left\{\left[\left(n - \frac{1}{n^2}\right)^2 \frac{\lambda_T'^2}{4} + \lambda_T'\right]^{\frac{1}{2}} - \frac{\lambda_T'}{2}\left(n - \frac{1}{n^2}\right)\right\}\right), \tag{14}$$

which enabled us to construct the diagram in Fig. 9, representing λ_T' as the function of θ and n.

The labyrinth factor, λ_T', defined in this way has the following features:

a. It can be higher than unity in the region of high porosity.

b. It extends from zero for $n = \infty$ to some upper definite value, which is attained with different values of n, depending on θ.

c. Above the curve for $n = 1$ there is a region of overlapping, i.e., every point in this region corresponds to at least two values of n.

It is obvious that every λ_{exp}' fits the model formally, if the condition (b) is fulfilled, for we can always find a value of n (for given θ), which gives $\lambda_T' = \lambda_{exp}'$.

We are now considering three parameters: λ_T', θ and $n = \rho/R$. Confirmation of the model really requires independent experimental determination of each of mentioned parameters, followed by comparison with corresponding theoretical values; this is not possible, even now. In this respect

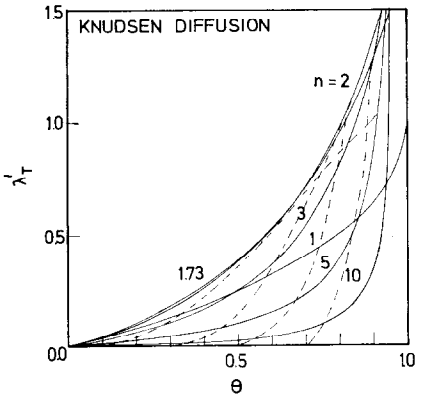

FIG. 9. Theoretical labyrinth factor for Knudsen diffusion vs total porosity, for different values of n; (– –) case I.

let us note that the parameter n is not a measurable property, owing to the fact that ρ does not exist as a real physical parameter, but represents in a way the mean value taken for all the pores with dimensions greater than R. Hence the simple measurement and comparison are not sufficient to confirm the consistency of the model and we must try some other way.

Formerly (*12*) we have shown that the variation in porosity from pellet to pellet of the same sample is caused primarily by the different weight (quantity of the solid phase) of pellets, the difference of pellet volume being of minor importance. On the other hand the variation in pore dimensions is undoubtedly directly influenced by the porosity variation (*21*). The same could be concluded for the results presented here, taking into account the functional relation between Knudsen diffusivity and pore dimensions.

With a view to describing theoretically the results obtained, we may consider two limiting behaviors of a porous pellet during the process of tableting.

In the first limiting case we assume that the packing of primary particles is rather close, resembling approximately the situation in Fig. 7. Variations in tableting pressure cause different deformations of the elementary cell in every pellet, such that R and ρ are each changed to the same extent (in one cell) from their mean values which correspond with the total assembly of pellets. In other words, the total volume of the elementary cell is different in different pellets, but its form remains unchanged. The deformations influence the pore volume of the cell, but their mass content remains constant from pellet to pellet.

The second limiting case resembles the situation of loosely packed spheres. Now we may expect that the average coordination number of spheres is less than 6, which number corresponds to the case in Fig. 7, i.e., some spheres are missing from the matrix of elementary cells. The most probable expectation is that the variation in tableting pressure causes primarily the rearrangement of spheres, and not their plastic deformation. The whole system subjected to pressure tends to the state in Fig. 7. Consequently, the changes include only the variation in magnitude of the central cubical pore of the cell, i.e., the variation only of the parameter ρ. Simplifying the situation we assume that the total volume of the elementary cell remains constant, but with variable mass content from pellet to pellet.

For a given assembly of porous pellets of the sample we can find experimentally the mean values of R and θ, i.e., R_0 and θ_0. Now we postulate the existence of the corresponding mean values of parameters n, ω and λ_T', i.e., n_0, ω_0 and λ_{T_0}', which are not directly measurable.

Case I. Constant Mass Content of the Elementary Cell

The change $\theta_0 \rightarrow \theta_i$ is accompanied by the corresponding changes $R_0 \rightarrow R_i$ and $\rho_0 \rightarrow \rho_i$. We may denote $X_i = R_i - R_0 = \rho_i - \rho_0$, and $\delta X_i = X_i/R_0$. The condition of constant mass content of the cell is fulfilled if

$$\frac{a_i}{a_0} = \left(\frac{1 - \theta_0}{1 - \theta_i}\right)^{\frac{1}{3}}. \tag{15}$$

Now, for a given value of X_i, we have

$$\omega_i = \frac{R_0 + X_i}{a_i} = \frac{R_0}{a_i}(1 + \delta X_i)\frac{a_0}{a_0}$$

$$= \omega_0(1 + \delta X_i)\left(\frac{1 - \theta_i}{1 - \theta_0}\right)^{\frac{1}{3}}, \tag{16}$$

$$n_i = \frac{\rho_0 + X_i}{R_0 + X_i}\cdot\frac{R_0}{R_0} = \frac{n_0 + \delta X_i}{1 + \delta X_i}.$$

Case II. Constant Volume of the Elementary Cell

The change $\theta_0 \rightarrow \theta_i$ is accompanied by the corresponding change $\rho_0 \rightarrow \rho_i$. R and a

remain constant, and equal to R_0 and a_0, respectively. For a given $X_i = \rho_i - \rho_0$, and corresponding $\delta X_i = X_i/R_0$, we have

$$\omega_i = \omega_0,$$

$$n_i = \frac{\rho_0 + X_i}{R_0} = n_0 + \delta X_i. \qquad (17)$$

Starting from θ_0 and D_{keff_0} we may construct the theoretical curves which correspond to the cases I and II, and compare them with experimental data, using the following procedure:

1. θ_0, D_{keff_0} and R_0 are experimentally determined (R_0 is the maximum in the pore volume distribution).
2. D_{kR_0} is calculated using $R = R_0$ in Eq. (10).
3. $\lambda_{exp_0}' = D_{keff_0}/D_{kR_0}$ is calculated.
4. n_0 is calculated from Eq. (14).
5. ω_0 is calculated using Eq. (5).
6. X_1 is chosen, and ω_1 and n_1 calculated according to Eq. (16) (case I), or Eq. 17 (case II); the corresponding values of θ_1 and λ_{T_1}' are also calculated using Eqs. (5) and (12), respectively; D_{keff_1} is calculated according to:

$$D_{keff_1} = 4850R_0(1 + \delta X_1)\cdot(T/M)^{\frac{1}{2}}\cdot\lambda_{T_1}' \quad \text{(case I)}.$$

$$D_{keff_1} = 4850R_0(T/M)^{\frac{1}{2}}\cdot\lambda_{T_1}' \quad \text{(case II)}.$$

7. The values of D_{keff_1} and θ_1 are plotted in the diagram D_{keff}–θ, containing also the experimental results.
8. Points (6) and (7) of the procedure are repeated with different values of X_i.

The procedure described has been carried out for each sample investigated. The curves in Figs. 3, 4, 5, 6, marked with I and II refer to the calculated values for cases I and II.

Sample No. 3 (Topsøe SK) is characterized by a bimodal distribution (Fig. 2). Hence the calculation in this case has been based on the mean value of the macropore diameter. As shown (Fig. 5), this procedure is justified.

From Figs. 3, 4, 5, and 6 it is clear that case I has advantage in representing the experimental results. This could have been expected in advance on the basis of the results of recent investigations of powder compaction (*22*). However, the dispersion of the experimental data is of such a character that the occurrence of case II cannot be totally excluded. We may safely conclude that the process of powder compaction includes both of the described mechanisms, the first one (plastic deformation of particles) being dominant.

The model presented here cannot predict the diffusivities, starting from the data on porosity and pore distribution, because we have no knowledge *a priori* about the parameters n or ρ, these two being inaccessible to direct measurement. Nevertheless, the model does not lose its physical sense because of that. To assert this we shall use the data presented by Currie (*4*) which have been obtained in the region of normal diffusion.

Similarly to Eq. (6), the effective pore dimension for the case of normal diffusion can be written as:

$$\frac{a}{a_{neff}^2} = \frac{a - \rho}{R^2} + \frac{\rho}{\rho^2}, \qquad (18)$$

and the labyrinth factor for normal diffusion, analogously to Eq. (9):

$$\lambda_n = \left(\frac{a_{neff}}{a}\right)^2 = \frac{\omega^2}{1 - \omega[n - (1/n)]}. \qquad (19)$$

Using Eqs. (19) and (5) we can construct a diagram, shown in Fig. 10, similar to that (Fig. 9) for Knudsen diffusion. In Fig. 10 there are also four experimental curves D_{12eff}/D_{12}–θ, according to Currie (*4*). Curve I, being obtained for glass spheres, sand, carborundum and NaCl, is characterized by a value of n from 1.73 to 2. It supports

very well the idea of approximately rounded particles of unconsolidated powder.

Curve IV, another extreme, has been obtained for vermiculite, mica and steel wool, all of them highly asymmetrical particles (vermiculite and mica—laminar particles or flakes; steel wool—long fibers), so we can expect high values of n, presupposing major differences in the pore dimensions of such material. Actually the obtained values of n are about 9.

Curves II (soil crumbs) and III (pumice, talc, kaolin and Celite), obtained for less definable materials, are situated between these two extremes.

Here we pay attention to the point that the experimentally obtained curves have the same trend as the calculated curves $\lambda_n = f(n, \theta)$, justifying the high degree of physical reality of the model. On the other hand, it is clear that the form of the primary particles has a most important influence, along with porosity, on the predicting of the labyrinth factor or diffusivity. This of itself emphasizes the need for much more experimental material in this field, if we wish to make reasonably good correlation between the form of the particles and n.

Nevertheless, combining this and the previous investigation (*12*), we can draw the following useful conclusions:

A. For given n and θ, the labyrinth factors for Knudsen and normal diffusion are not in general equal. From Eqs. (12) and (19) we obtain the ratio

$$\frac{\lambda_T'}{\lambda_n} = 1 + \frac{(\omega/n)[1 - (1/n)]}{1 - \omega[n - (1/n^2)]}. \quad (20)$$

For n = constant, this ratio rises with ω, i.e., with porosity, and ranges from 1 ($\theta = 0$) to n ($\theta = 1$). In the case of ω = constant, the ratio becomes unity for $n = 1$ and $n = \infty$, and between these two values for n, there exists a maximum, the position of which is a function of θ; the higher the porosity, the higher the n at which the maximum is attained. This is in accordance with the phenomenon of overlapping mentioned above.

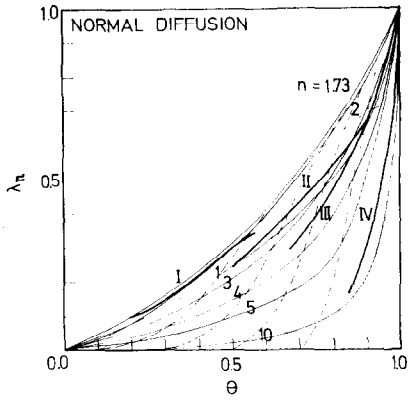

FIG. 10. Theoretical labyrinth factor for normal diffusion vs total porosity, for different values of n; (– –) case I. (I, II, III, IV) Experimentally obtained curves, according to Currie (4) (see text).

Finally, disregarding the theoretical values of the ratio (*20*), in the majority of real cases values higher than 2 are not to be expected;

B. Using data (*12*) on the porosity variation in dependence on the mean absolute porosity of the sample (based on 6 commercial samples with θ_0 ranging from about 0.3 to about 0.7, 263 pellets in all), it is possible to estimate the degree of the variation of the labyrinth factor of the sample.

The porosity variation of the sample is given by (*12*):

$$V(\theta) = \frac{1 - \theta_0}{\theta_0}[V^2(g) + V^2(V)]^{\frac{1}{2}}, \quad (21)$$

the mean value of the square root being 6.55. The standard deviation of porosity is now:

$$S(\theta) = 0.0655(1 - \theta_0). \quad (22)$$

If we assume, after the model presented, that the variation of the labyrinth factor occurs along the broken lines in Fig. 9 (describing case I of the model), we can easily obtain the variation of the labyrinth factor from the porosity variation of the

sample. The lines analogous to the broken ones can be constructed starting from any point in the diagram, following the procedure for case I.

Proceeding in this way, we note that the variation of the labyrinth factor of the sample depends primarily on the slope of the broken curves, which depends on the "level" of the labyrinth factor, or on the mean value for the sample. The influence of θ_0 is of minor importance. Thus for

$\lambda_0 = 0.01$ we have $V(\lambda) =$ about 100%,

$\lambda_0 = 0.1$ $V(\lambda) =$ 30–50%,

$\lambda_0 = 0.5$ $V(\lambda) =$ 10–20%.

The greater variations correspond with greater porosity.

In the case of normal diffusion the variation of labyrinth factor is respectively less emphasized, due to the more gentle slope of the broken lines (Fig. 10).

The results of this estimate must especially be kept in mind when speculating with low values of effective diffusivity (i.e., low level of labyrinth factor), obtained as the mean value for several pellets in a single experiment.

ACKNOWLEDGMENTS

The presented work, which is part of a major project on the fundamental aspects of heterogeneous catalysis, has been supported by the Funds for Scientific Research of SR Srbija. The author is also grateful to Mr. Žarko Jovanović of the Dept. of Catalysis for supplying the sample Ž-46.

REFERENCES

1. Wheeler, A., *in* "Advances in Catalysis" (W. G. Frankenburg, V. I. Komarewsky, E. K. Rideal, P. H. Emmett, H. S. Taylor, Eds.), Vol. III, p. 249. Academic Press, New York, 1951.
2. Petersen, E. E., *AIChE J.* **4**, 343 (1958).
3. Michaels, A. S., *AIChE J.* **5**, 270 (1959).
4. Currie, J. A., *Brit. J. Appl. Phys.* **11**, 318 (1960).
5. Weisz, P. B., and Schwartz, A. B., *J. Catal.* **1**, 399 (1962).
6. Wako, N., and Smith, J. M., *Chem. Eng. Sci.* **17**, 825 (1962).
7. Johnson, M. F. L., and Stewart, W. E., *J. Catal.* **4**, 248 (1965).
8. Foster, R. N., and Butt, J. B., *AIChE J.* **11**, 180 (1966).
9. Satterfield, C. M., "Mass Transfer in Heterogeneous Catalysis," p. 71, M.I.T. Press, Cambridge, Mass., 1970.
10. Foster, R. N., Butt, J. B., and Bliss, H., *J. Catal.* **7**, 179, 191 (1967).
11. Wicke, E., and Kallenbach, R., *Kolloid. Z.* **97**, 135 (1941).
12. Smiljanić, D., *Hemijska Industrija* **6**, 251 (1974).
13. Villet, R. H., Wilhelm, R. H., *Ind. Eng. Chem.* **53**, 837 (1961).
14. Putanov, P., and Smiljanić, D., *Proc. I Congr. Chem. Eng. Proc. Techn.*, p. 279. Savez inženjera i tehničara tehnologa i hemičara Srbije, Beograd, 1971.
15. Pátý, L., "Fyzika nízkých tlaku," p. 62. Academia, Prague, 1968.
16. Present, R. D., "Kinetic Theory of Gases," p. 63. McGraw-Hill, 1958.
17. Hudgins, R. R., Kadlec, B., and Silveston, P. L., *J. Catal.* **32**, 237 (1974).
18. Ref. (*9*), p. 34.
19. Dushman, S., "Scientific Foundations of Vacuum Technique," 2nd ed., Chap. 2. Wiley, New York, 1962.
20. Ferraiolo, G., Merli, C., and Reverberi, A., *Ann. Chim.* **57**, 240 (1967).
21. Rao, R. M., Wakao, N., and Smith, J. M., *Ind. Eng. Chem. Fundam.* **3**, 127 (1964).
22. Gray, W. A., "The Packing of Solid Particles," pp. 95–96. Chapman and Hall, London, 1968.